Electronic Supplementary Material (ESI) for Inorganic Chemistry Frontiers.


# Application of Changing the Valence State of Metal Through Reaction Time to Efficient Oxygen Evolution Reaction

Ming Chen[a], Sha Luo[b], Zongyan Ma[a], Fei Yuan[a], Jing Chen[a], Linkun Dong[a], Weiwen Mao[a] and Jiantai Ma*[a]

a. State Key Laboratory of Applied Organic Chemistry (SKLAOC), Gansu Provincial Engineering Laboratory for Chemical Catalysis, College of Chemistry and Chemical Engineering, Lanzhou University, Lanzhou, 730000, PR China.

b. School of Materials and Energy, University of Electronic Science and Technology, Chengdu, China

Corresponding Autor, Jiantai Ma*; E-mail address: majiantai@lzu.edu.cn (J. Ma)

## Experiment section

## Materials and chemicals

Iron (III) chloride hexahydrate ($FeCl_3$•$6H_2O$, CP, ≥98.0%) was purchased from Chengdu Kelong Chemical Co., Ltd. Nickel (II) chloride hexahydrate ($NiCl_2$•$6H_2O$, AR, ≥98.0%) was purchased from Beijing Hongxing Co. Ltd. The type of CNTs was TNM5 (external diameter: 20–30 nm, length:10–30 mm, ≥98% w/w), which was purchased from Chengdu Organic Chemicals Co., Ltd. Chinese Academy of Sciences. Sodium sulfide nonahydrate ($Na_2S$•$9H_2O$, AR, ≥98.0%) was purchased from Tianjin Damao Co. Ltd. Deionizedwater (18.2 MΩ) was used throughout the experiment. Pt/C (20 wt%) and Nafion (5 wt%) were supplied by Alfa Aesar. In addition, all of regents in this study were not further purified before used.

## Characterization

The morphologies of FeNiS/CNTs were observed using field emission scanning microscopy (SEM, HITACHI S-4800). Transmission electron microscope (TEM) images were observed with a Tecnai$^{TM}$ G$^2$F30, FEI operating at 200 kV, equipped with energy dispersive X-ray spectroscopy (EDX, Tecnai G2, NLD). The powder X-ray diffraction (XRD) were conducted by using Cu-Kα radiation as the X-ray source in the $2\theta$ range of 5-90°. X-ray photoelectron spectroscopy (XPS) was performed using a Kratos AXIS Ultra DLD instruments with a monochromatic X-ray source (AL Kα hν = 1486.6) and all elemental peaks were revised by the standard position of C 1s peak. The Brunauer-Emmett-Teller (BET) specific surface areas were calculated based on the nitrogen sorption isotherms obtained on a Micromeritics ASAP 2460 volumetric adsorption apparatus at 77 K. The results of Inductively Coupled Plasma Optical Emission Spectrometry (ICP-OES) were measured using an instrument model Plasma Quant PQ9000.

## Electrochemical measurement

Generally, 4.5 mg catalyst powder was dissolved in a 1 mL of solution which was composed of ethanol and ultrapure water in a 1:1 volume ratio. Then, ultrasonic treatment was performed for more than 0.5 h to form a uniform black solution. Eventually, 5.5 μl black solution and 3 μl nafion aqueous solution (0.5 wt%) were dropped on the 3.0 mm diameter glassy carbon electrode serving as the working electrode. In this study, all the electrochemical tests were realized through electrochemical workstation (CHI 660E, Shanghai Chenhua) with three-electrode configuration without iR compensation and at room temperature. In the test, a graphite

carbon rod was utilized as contrast electrode, while the saturated Ag/AgCl electrode was treated as the reference electrode. All potentials (vs. Ag/AgCl) appearing in the article were transformed into reversible hydrogen electrode (RHE), which were corrected by means of using the Nernst equation: E (vs. RHE) = E (vs. Ag/AgCl) + 0.059 pH + 0.198 V.

## OER measurement

The OER electrochemical activities were all measured in 1.0 M KOH electrolyte. Linear sweep voltammetry (LSV) polarization curves were investigated in the range of -0.3 V – 0.7 V vs. Ag/AgCl with a scan rate of 5 mV $s^{-1}$. The EIS value was obtained through testing under the potential of OER response after the open-circuit voltage stabilized. Its bias setting always corresponds to the potential at the current density of 10mA $cm^{-2}$, and the measured frequency range is $10^5$ to 0.01Hz. In order to obtain the electrochemically active surface areas of all the catalysts, cyclic voltammograms (CVs) were investigated between 0.2 V and 0.3 V with the different scan rates (10-100 mV $s^{-1}$). In addition, the OER stability of the catalysts was also performed by Amperometric i-t Curve at 10 mA $cm^{-2}$ vs. RHE. All the current density of the catalysts were rectified to the geometrical surface area of the GCE (0.07 $cm^{-2}$).

## Calculation of TOF

The TOF values of catalysts were calculated through the following equation:

$$TOF\ (s^{-1}) = (j \times A) / (4 \times F \times n)^1$$

Where j (A $cm^{-2}$) is the current density at a given overpotential, A = 0.7 $cm^2$ is the geometric surface area of the electrode, F = 96500 C $mol^{-1}$ stands for the Faraday constant, n (mol) is mole number of transition metal(s) loaded on the GC electrode which was determined by the ICP-OES analysis. All metal cations in the catalysts were assumed to be catalytically active, so the calculated values represents the lower limits of TOF.

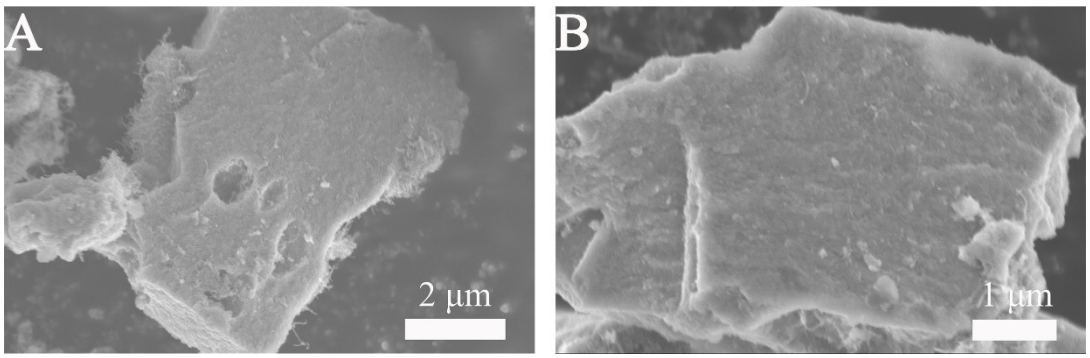


Figure S1 SEM images of NiFeS/CNTs.

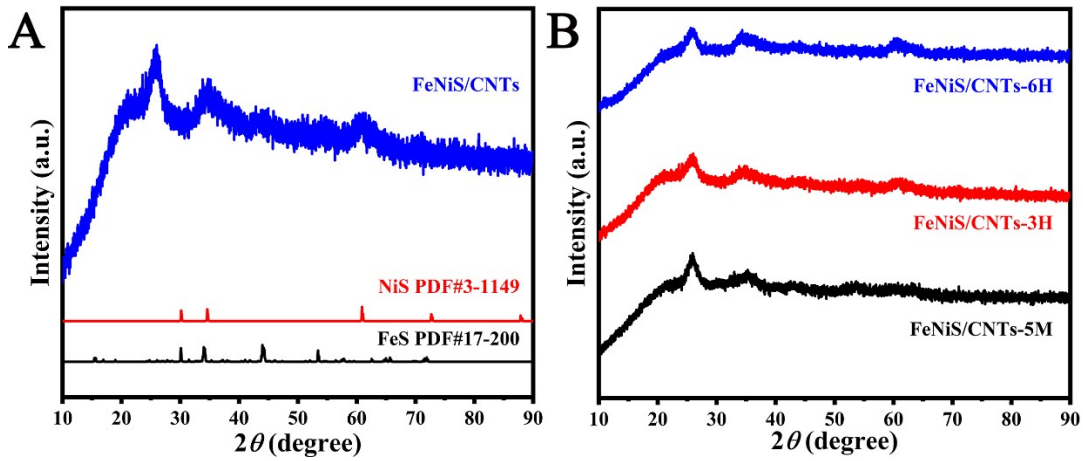


Figure S2 (A) The XRD spectra of FeNiS/CNTs, (B) The XRD spectra of FeNiS/CNTs-5M, FeNiS/CNTs-3H and FeNiS/CNTs-6H.

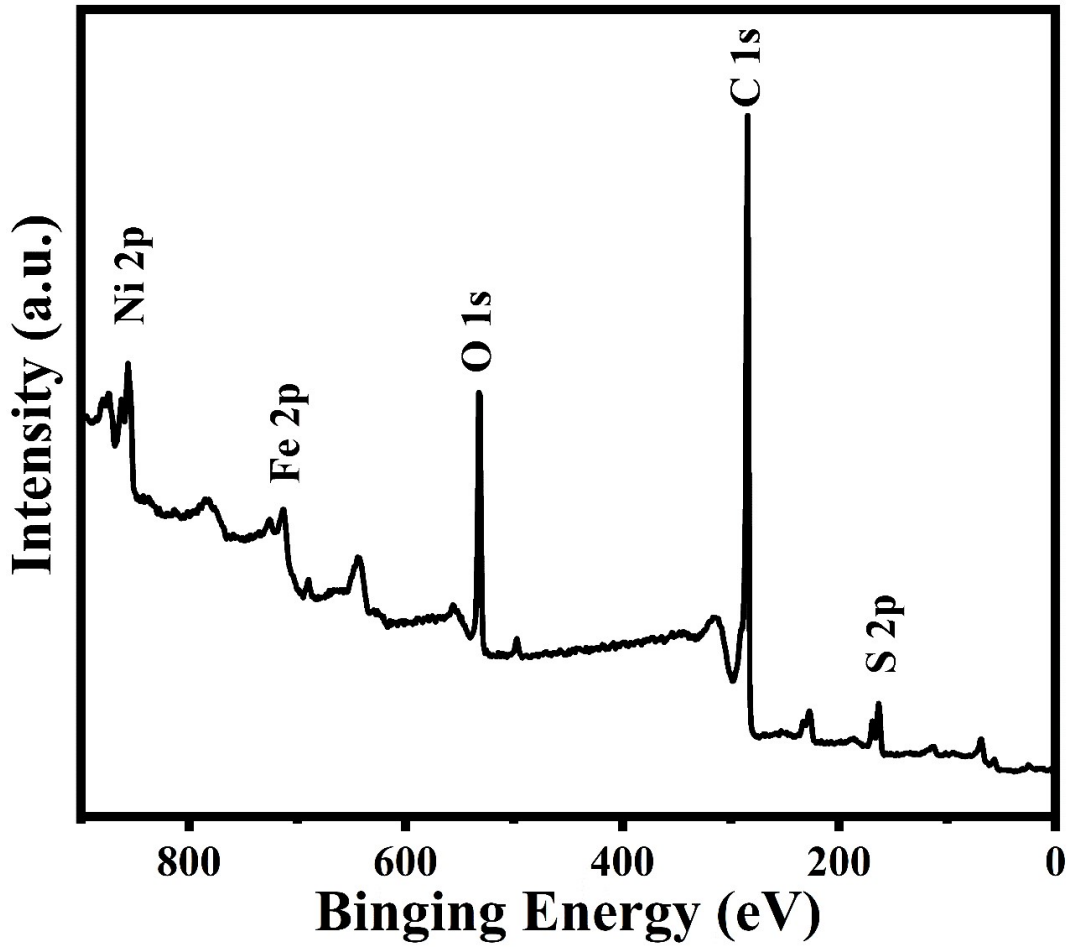


Figure S3 XPS wide spectra of FeNiS/CNTs.

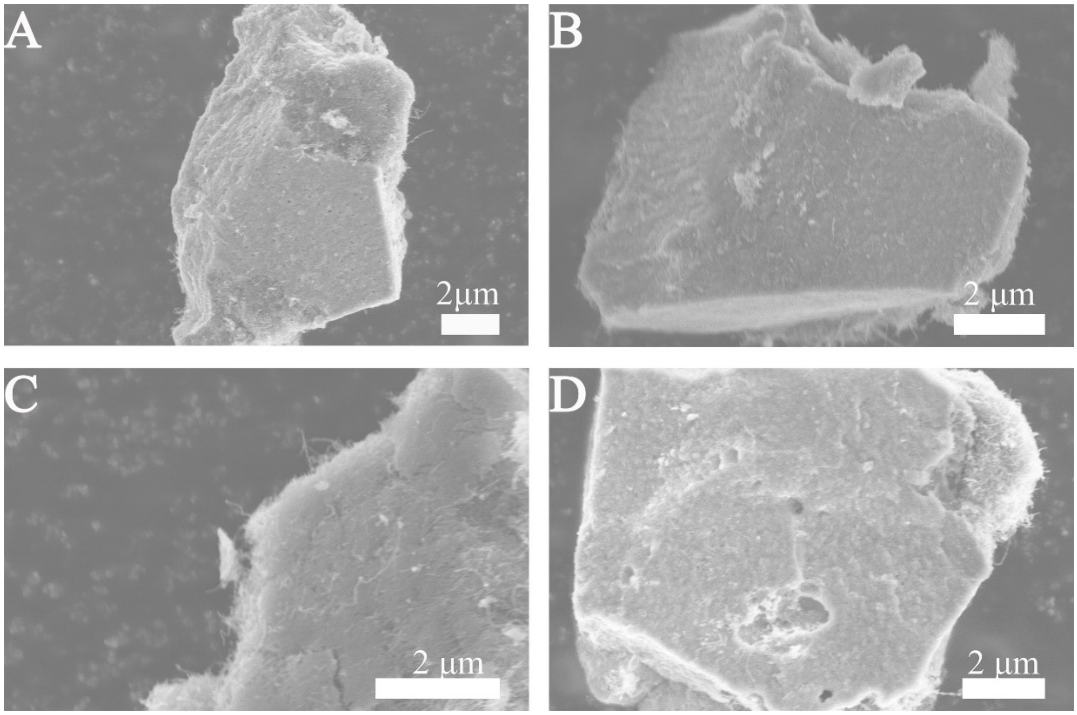


Figure S4 SEM images of (A) (B) NiFeS/CNTs-5M and (C) (D) NiFeS/CNTs-6H.

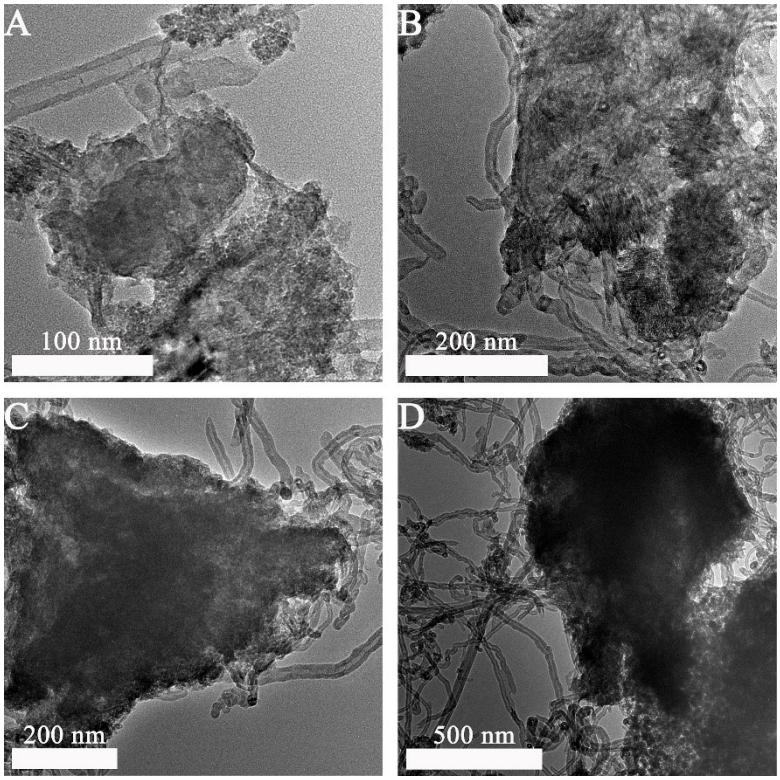


Figure S5 TEM images of (A) (B) NiFeS/CNTs-5M and (C) (D) NiFeS/CNTs-6H.

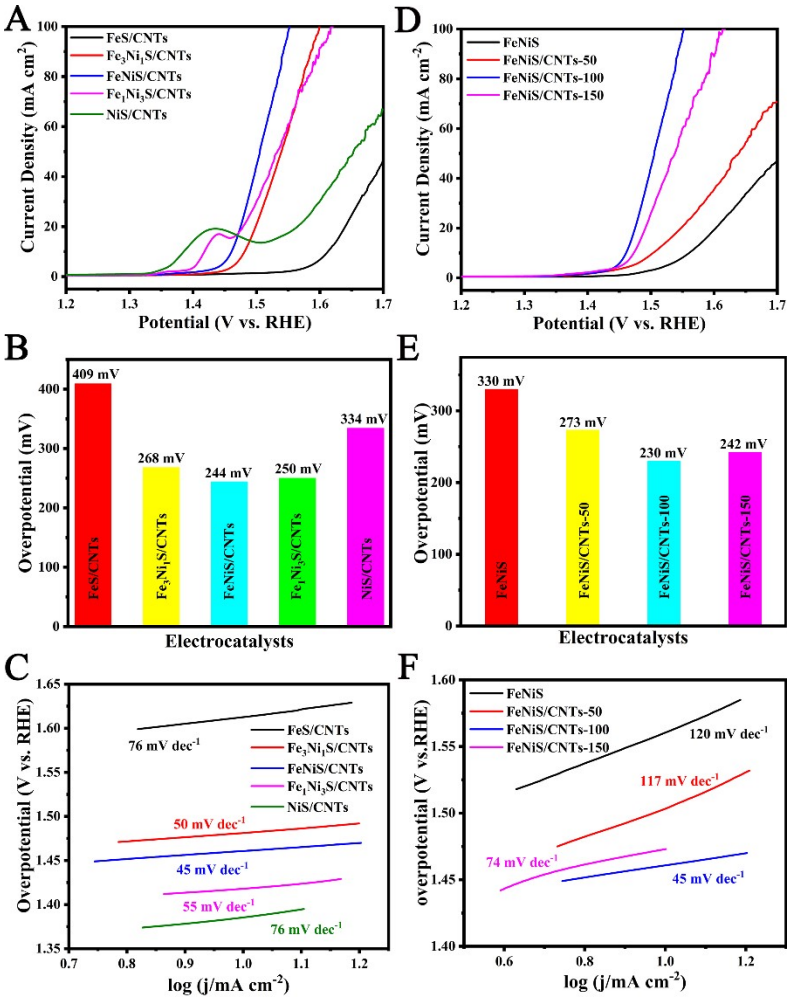


Figure S6 (A) LSV curves, (B) Tafel slopes, and (C) corresponding overpotentials at 10 mA $cm^{-2}$ of FeS/CNTs, $Fe_3Ni_1S$/CNTs, FeNiS/CNTs, $Fe_1Ni_3S$/CNTs and NiS/CNTs; (D) LSV curves, (E) Tafel slopes, and (F) corresponding overpotentials at 10 mA $cm^{-2}$ of FeNiS, FeNiS/CNTs-50, FeNiS/CNTs-100 and FeNiS/CNTs-150.

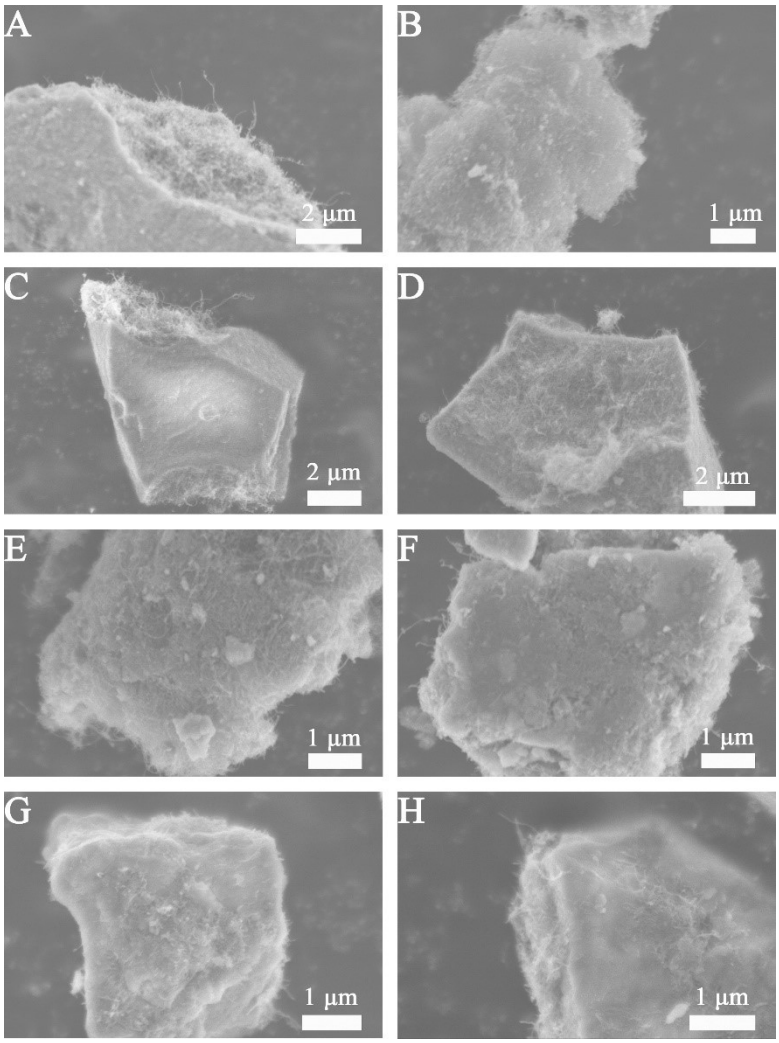


Figure S7 SEM images of (A) (B) FeS/CNTs, (C) (D) NiS/CNTs, (E) (F) $Fe_3Ni_1S$-CNTs and (G) (H) $Fe_1Ni_3S$-CNTs.

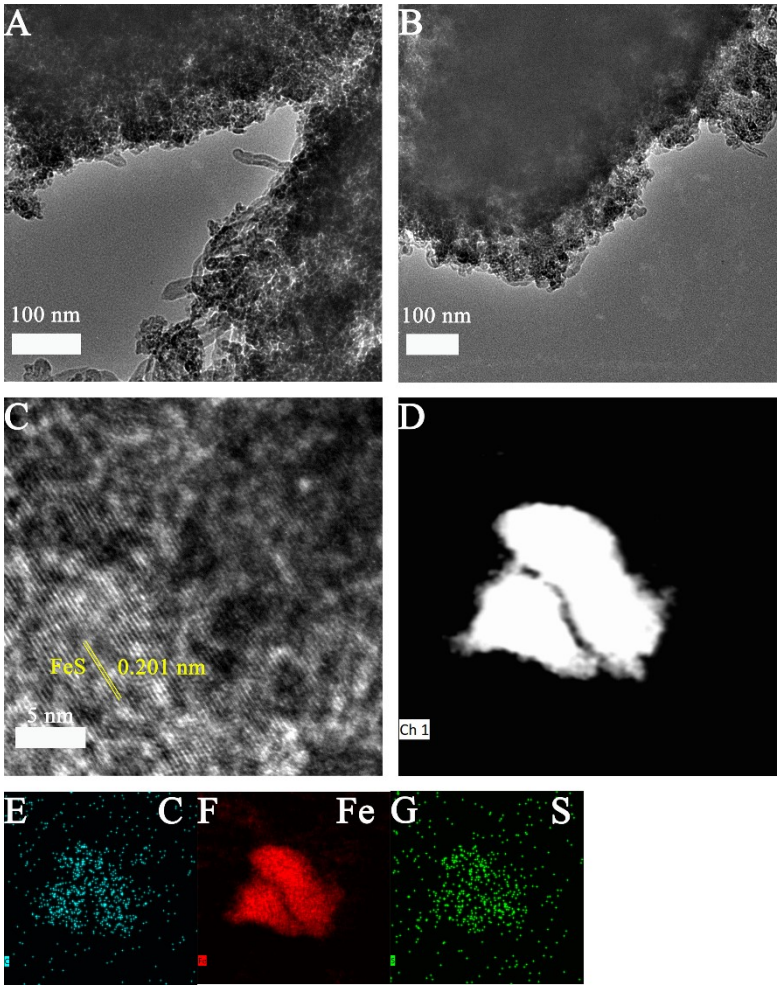


Figure S8 (A) and (B) TEM images of different positions of FeS/CNTs, (C) HRTEM of FeS/CNTs, (D) Dark field TEM of FeS/CNTs, (E-G) EDS elemental mapping of the FeS/CNTs refers to the signals of C, Fe and S respectively.

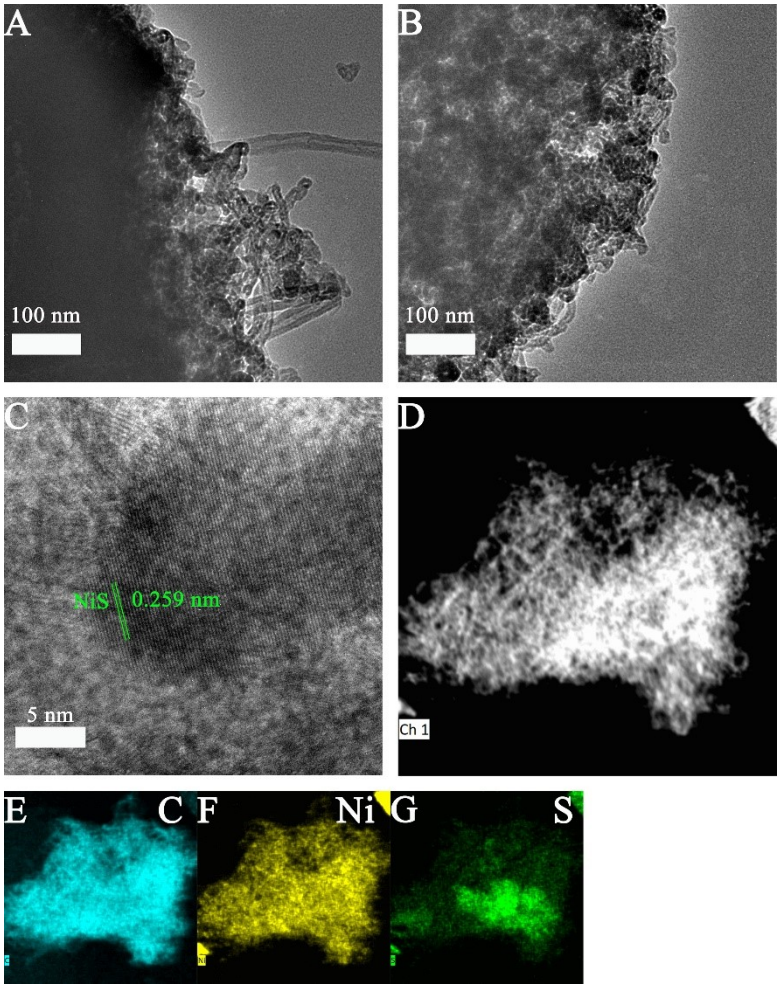


Figure S9 (A) and (B) TEM images of different positions of NiS/CNTs, (C) HRTEM of NiS/CNTs, (D) Dark field TEM of NiS/CNTs, (E-G) EDS elemental mapping of the NiS/CNTs refers to the signals of C, Ni and S respectively.

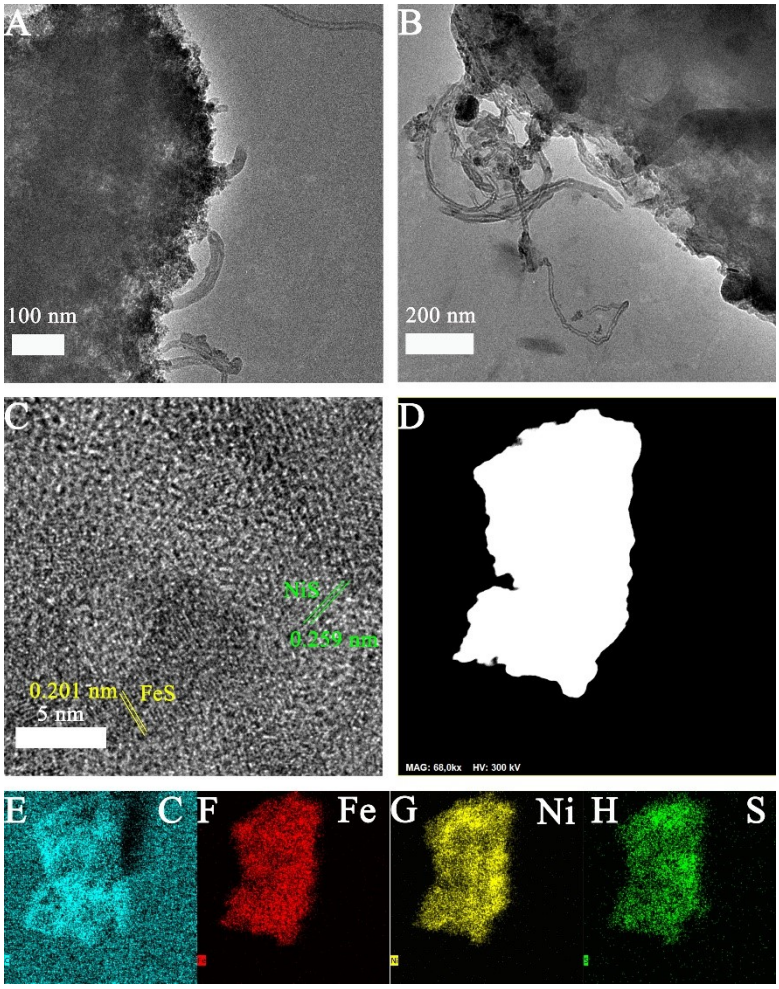


Figure S10 (A) and (B) TEM images of different positions of $Fe_3Ni_1S$/CNTs, (C) HRTEM of $Fe_3Ni_1S$/CNTs, (D) Dark field TEM of $Fe_3Ni_1S$/CNTs, (E-G) EDS elemental mapping of the $Fe_3Ni_1S$/CNTs refers to the signals of C, Fe, Ni and S respectively.

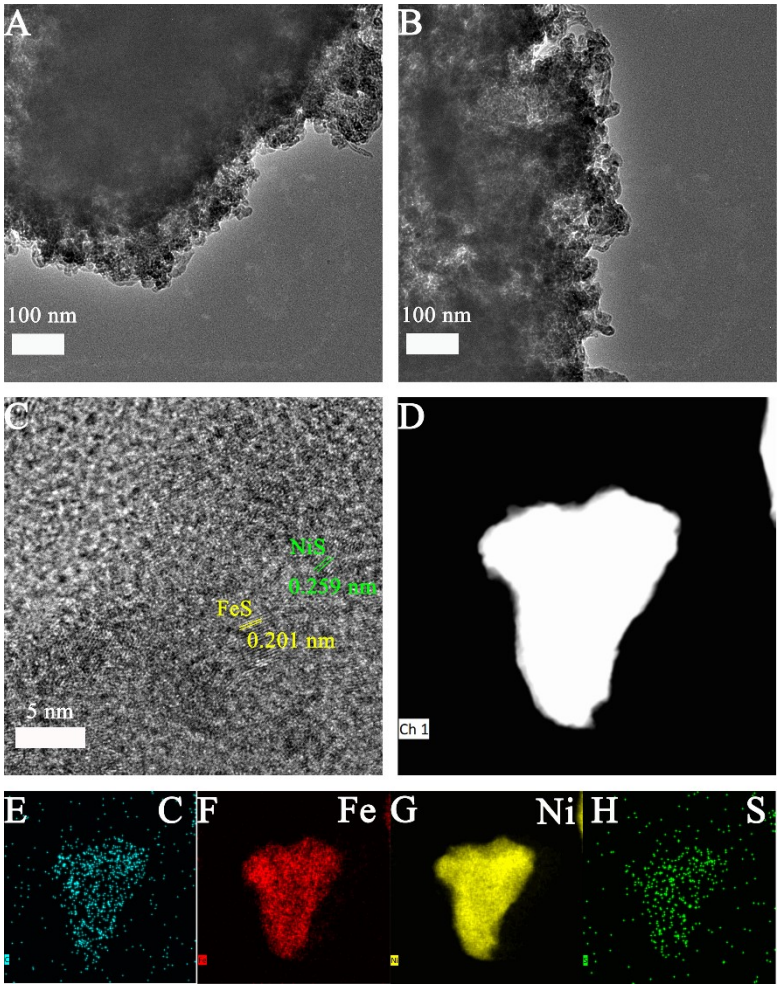


Figure S11 (A) and (B) TEM images of different positions of $Fe_1Ni_3S$/CNTs, (C) HRTEM of $Fe_1Ni_3S$/CNTs, (D) Dark field TEM of $Fe_1Ni_3S$/CNTs, (E-G) EDS elemental mapping of the $Fe_1Ni_3S$/CNTs refers to the signals of C, Fe, Ni and S respectively.

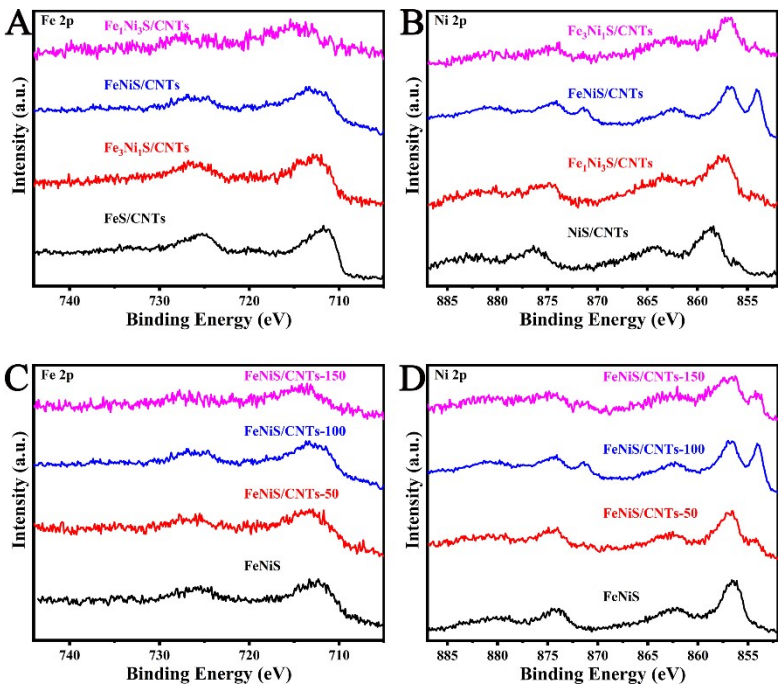


Figure S12 XPS spectra of catalysts with different metal ratios: (A) Fe 2p and (B) Ni 2p; XPS spectra of catalysts with different CNTs content: (C) Fe 2p and (D) Ni 2p.

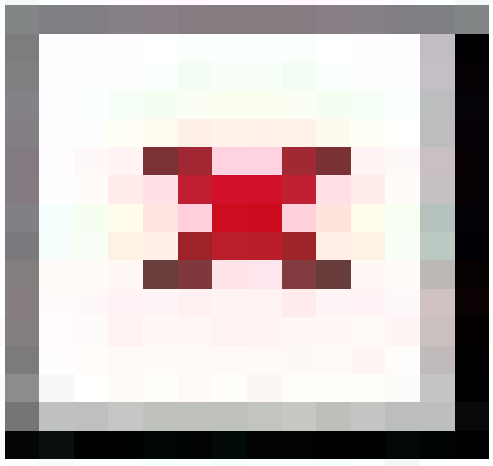

Figure S13 Zeta Potential of catalysts with different CNTs content.

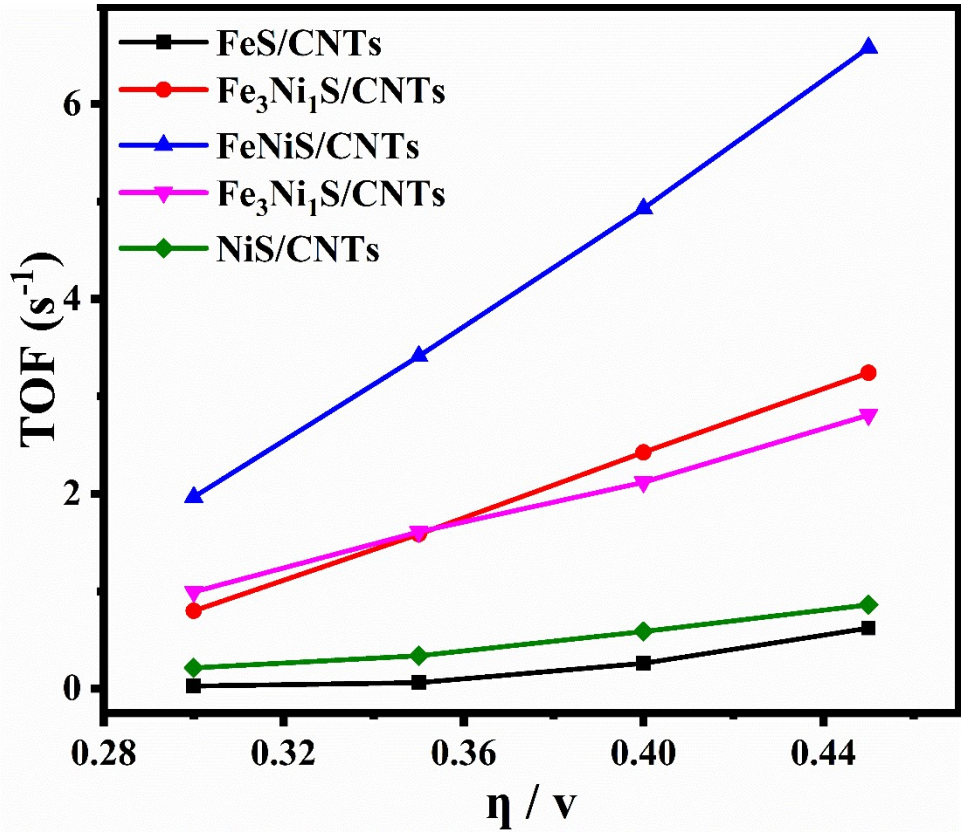


Figure S14 TOF values calculated at η = 300, 350, 400 and 450 mV

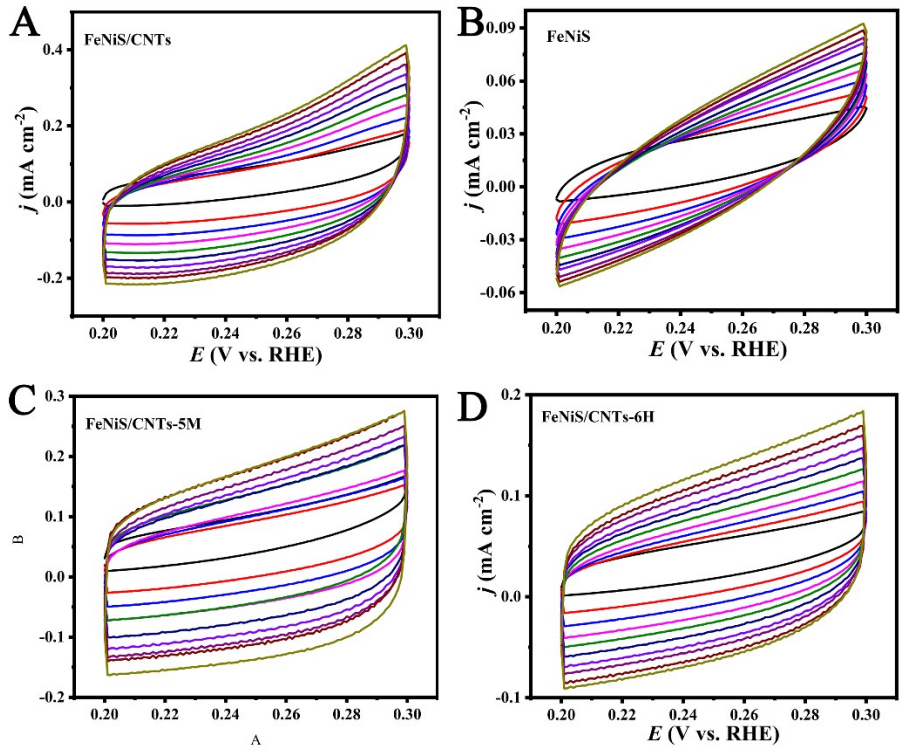


Figure S15 CV curves of (A) FeNiS/CNTs (b) FeNiS (c) FeNiS/CNTs-5M (d) FeNiS/CNTs-6H

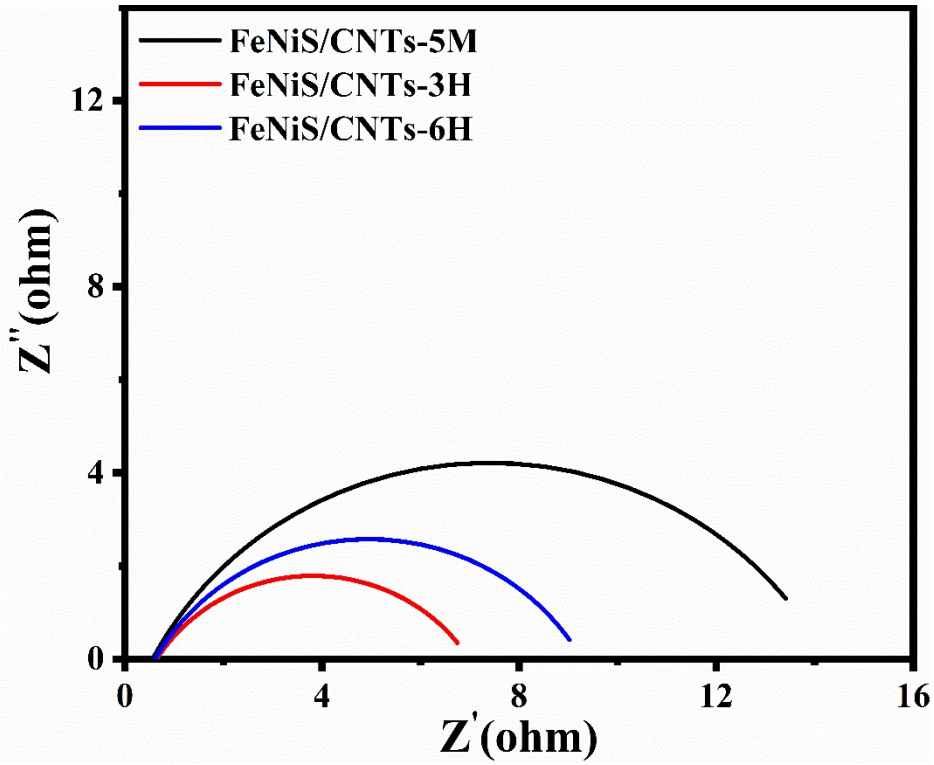


Figure S16 Nyquist plots of FeNiS/CNTs-5M, FeNiS/CNTs-3H and FeNiS/CNTs-6H.

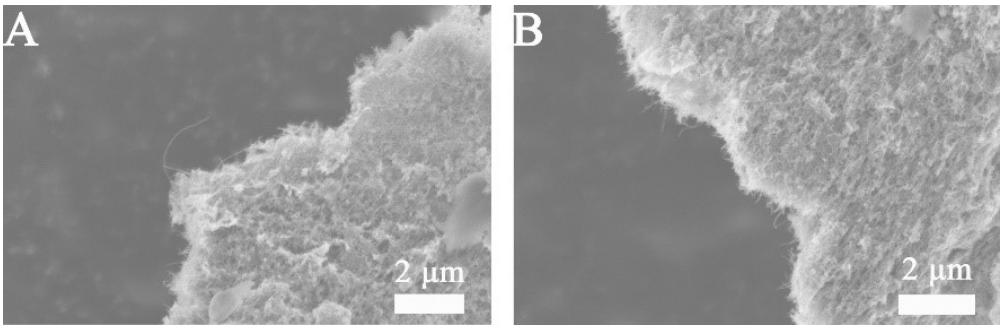


Figure S17 SEM images of the FeNiS/CNTs after IT test.

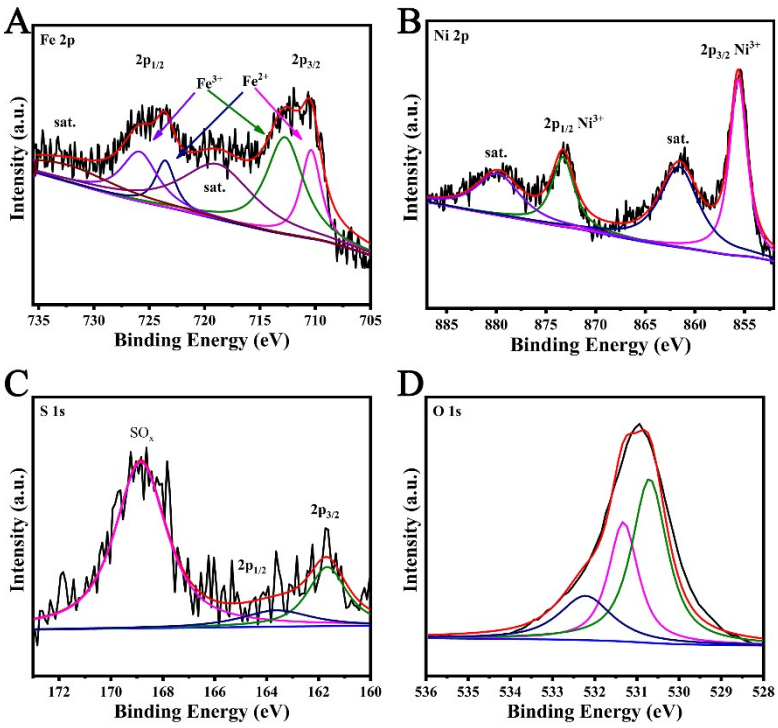


Figure S18 XPS spectra of the FeNiS/CNTs after IT test: (A) Fe 2p, (B) Ni 2p, (C) S 1s and (D) O 1s.

Table S1 The comparison of OER performance between metal sulfide catalysts in alkaline media

| Catalysts | Overpotential (mV) @ 10 mA cm-2 | Tafel slope (mV $dec^{-1}$) | Reference |
|---|---|---|---|
| FeNiS/CNTs | 230 | 45 | This work |
| CoS-5 | 290 | 66 | [2] |
| C-$Ni_3S_2$ | 261 | 95 | [3] |
| CoO@S-CoTe | 246 | 56 | [4] |
| FeS (A650) | 263 | 48 | [5] |
| pc-$Ni_3S_2$@CNF | 270 | 51 | [6] |
| CeNdS/$C_{60}$ | 346 | 68 | [7] |
| $NiCo_2S_4$/HCS-3 | 310 | 78 | [8] |
| NiS-M/NF | 255 | 76 | [9] |
| $Co_9S_8$-$Ni_3S_2$/NF-0.6 | 233 | 117 | [10] |
| $Ni_9S8/Ag_2S$ | 277 | 72 | [11] |

Table S2 The Integral table of Fe and Ni peak area in XPS data of catalysts with different reaction time and the catalyst after IT test.

| Samples | $Fe^{2+}/Fe^{3+}$ | | $Ni^{2+}/Ni^{3+}$ | |
|---|---|---|---|---|
| | 2p1/2 | 2p3/2 | 2p1/2 | 2p3/2 |
| FeNiS/CNTs-5M | 1.23 | 1.23 | 0.09 | 0.09 |
| FeNiS/CNTs-3H | 1.05 | 1.05 | 0.36 | 0.36 |
| FeNiS/CNTs-6H | 1.35 | 1.35 | 0.04 | 0.04 |
| FeNiS/CNTs after IT test | 0.50 | 0.50 | 0 | 0 |

Table S3 Metal contents of the catalysts analysed by ICP-OES

| Samples | Fe:Ni (initial molar ratio) | Fe:Ni actual amount (mmol) | Fe:Ni (actual molar ratio) |
|---|---|---|---|
| $Fe_3Ni_1S$/CNTs | 3 | $15.45*10^{-3}/5.26*10^{-3}$ | 2.94 |
| FeNiS/CNTs | 1 | $7.58*10^{-3}/7.02*10^{-3}$ | 1.08 |
| $Fe_1Ni_3S$/CNTs | 0.33 | $4.80*10^{-3}/13.28*10^{-3}$ | 0.36 |
| FeNiS/CNTs-50 | 1 | $9.2*10^{-3}/10.6*10^{-3}$ | 0.87 |
| FeNiS/CNTs-150 | 1 | $5.3*10^{-3}/5.6*10^{-3}$ | 0.95 |

1. J. Xu, J. Li, D. Xiong, B. Zhang, Y. Liu, K.-H. Wu, I. Amorim, W. Li and L. Liu, Trends in

activity for the oxygen evolution reaction on transition metal (M = Fe, Co, Ni) phosphide pre-catalysts, *Chem Sci*, 2018, **9**, 3470-3476.

2. Y. Zhang, G. B. Zheng, A. L. Li, X. K. Zhu, J. J. Jiang, Q. Zhang, L. W. Deng, X. H. Gao and F. P. Ouyang, Hexagonal Single-Crystal CoS Nanosheets: Controllable Synthesis and Tunable Oxygen Evolution Performance, *Inorg Chem*, 2022, **61**, 7568-7578.
3. X. Q. Zheng, L. Zhang, W. He, L. Li and S. Lu, Heteroatom-Doped Nickel Sulfide for Efficient Electrochemical Oxygen Evolution Reaction, *Energies*, 2023, **16**, 881.
4. X. Wang, Z. L. Mao, X. Mao, X. M. Hu, F. Y. Gao, M. R. Gao, Q. L. Wu, X. Lyu, A. J. Du, X. S. Xu, Y. Jia and L. Wang, Dual Integrating Oxygen and Sulphur on Surface of CoTe Nanorods Triggers Enhanced Oxygen Evolution Reaction, *Adv Sci*, 2023, **10**, 2206204.
5. R. Velmurugan, D. Amuthan, V. Saranyan and B. Subramanian, In situ moulded troilite 2H phase Fe S sultrathin electrodes via pulsed laser deposition for flexible solid state high capacity supercapacitor besides boosted electrocatalytic oxygen evolution reaction, *J Mater Chem A*, 2023, **11**, 5148-5165.
6. A. Tahir, T. ul Haq, F. Aftab, M. Zaheer, H. Duran, K. Kirchhoff, I. Lieberwirth and S. N. Arshad, Amorphous to Crystalline Ni3S2 Nanostructures Anchored on N-Doped Carbon Nanofibers for Electrochemical Splitting of Water, *Acs Appl Nano Mater*, 2023, **6**, 2336-2345.
7. T. Munawar, A. Bashir, M. S. Nadeem, F. Mukhtar, S. Manzoor, M. N. Ashiq, S. A. Khan, M. Koc and F. Iqbal, Electrochemical Performance Evaluation of Bimetallic Sulfide Nanocomposite with Fullerene (CeNdS/C60) for Efficient Oxygen Evolution Reaction (OER), *Energ Fuel*, 2023, **37**, 1370–1386.
8. J. Liu, X. Meng, J. H. Xie, B. Liu, B. Tang, R. Y. Wang, C. Wang, P. Gu, Y. D. Song, S. C. Huo and J. L. Zou, Dual Active Sites Engineering on Sea Urchin-Like CoNiS Hollow Nanosphere for Stabilizing Oxygen Electrocatalysis via a Template-Free Vulcanization Strategy, *Adv Funct Mater*, 2023, **33**, 2300579.
9. S. Ghosh, B. Dasgupta, S. Kalra, M. L. P. Ashton, R. T. Yang, C. J. Kueppers, S. Gok, E. G. Alonso, J. Schmidt, K. Laun, I. Zebger, C. Walter, M. Driess and P. W. Menezes, Evolution of Carbonate-Intercalated gamma-NiOOH from a Molecularly Derived Nickel Sulfide (Pre)Catalyst for Efficient Water and Selective Organic Oxidation, *Small*, 2023, **19**, 2206679.
10. Y. P. Bu, Y. W. Zhang, Y. Y. Liu, S. M. Li, Y. L. Zhou, X. F. Lin, Z. C. Dong, R. C. Zhang, J. C. Zhang and D. J. Zhang, MOF-Derived Urchin-like Co9S8-Ni3S2 Composites on Ni Foam as Efficient Self-Supported Electrocatalysts for Oxygen Evolution Reaction, *Batteries-Basel*, 2023, **9**, 46.
11. R. Biswas, I. Ahmed, P. Manna, P. Mahata, R. S. Dhayal, A. Singh, J. Lahtinen and K. K. Haldar, Facile Fabrication of Ni9S8/Ag2S Intertwined Structures for Oxygen and Hydrogen Evolution Reactions, *Chempluschem*, 2023, **88**, e202200320.